Effect of short chain branching on the interlamellar structure of semicrystalline polyethylene

by

Vaibhaw Kumar[1], C. Rebecca Locker[2], Pieter J. in 't Veld[3] and Gregory C. Rutledge[1,·]

[1]*Department of Chemical Engineering, Massachusetts Institute of Technology, 77 Massachusetts Ave, Cambridge, MA, 02139*

[2]*ExxonMobil Research and Engineering Company, 1545 Route 22 East, Annandale, New Jersey 08801, United States*

[3]*BASF SE, GME/MM, Carl Bosch Str. 38, 67056 Ludwigshafen, Germany*

Submitted to Macromolecules

· Electronic address: rutledge@mit.edu

Abstract

We use molecular simulations with a united atom force field to examine the effect of short chain branching (SCB) on the noncrystalline, interlamellar structure typical of linear low density polyethylene (LLDPE). The model is predicated on a metastable thermodynamic equilibrium within the interlamellar space of the crystal stack and accounts explicitly for the various chain topologies (loops, tails, and bridges) therein. We examine three branched systems containing methyl, ethyl, and butyl side branches, and compare our results to high density polyethylene (HDPE), without branches. We also compare results for two united atom force fields, PYS and TraPPE-UA, within the context of these simulations. In contrast to conventional wisdom, our simulations indicate that the thicknesses of the interfacial regions in systems with SCB are smaller than those observed for a linear polyethylene without branches, and that branches are uniformly distributed throughout the interlamellar region. We find a prevalence of gauche states along the backbone due to the presence of branches, and an abrupt decrease in the orientational order in the region immediately adjacent to the crystallite.

Introduction:

Linear low density polyethylene (LLDPE) is one of the most popular plastic grades used in the film and packaging industry, due to its great flexibility and high tear resistance. The presence of short chain branching (SCB) along the carbon backbone is responsible for these exceptional properties of LLDPE. With the advancement in chemical synthesis methods and invention of new catalysts, it is now possible to synthesize LLDPE with great control over both the extent and length of branching. Greater control over branching permits the realization of properties intermediate between those of conventional high and low density polyethylenes, and has resulted in the production of a wide variety of LLDPE-based products whose material properties can be fine-tuned. Increased demand for LLDPE-based materials motivates closer examination of the structure-property relations among this class of polymers.

The presence of SCB can have a significant influence on the semicrystalline morphology, which in turn affects the macroscopic properties of the semicrystalline material. Voigt-Martin et al.[1] used transmission electron microscopy (TEM) to analyze the lamellar structure of semicrystalline polymers containing ethyl, hexyl, and acetate side chains. Defoor et al.[2] also used TEM to examine the structure of poly(ethylene-1-octene) (i.e. comprising hexyl branches) at branch densities ranging from 3-28 branches per 1000 C. Both of these groups observed decreases in the crystallite thickness and percentage crystallinity with increasing co-monomer content. Defoor et al.[2] also reported an increase in the interfacial thickness between crystalline and noncrystalline domains as the 1-octene co-monomer content was increased; however, the molecular weight (MW) of their samples also varied with the branch content, making it difficult to ascribe this trend to SCB unambiguously. Working with samples having narrow MW distributions, Alamo et al.[3] carried out an extensive study using Raman spectroscopy on ethylene copolymerized with 1-

butene (ethyl-branched), 1-hexene (butyl-branched), and 1-octene (hexyl-branched). They also reported a significant increase in the interfacial thickness for the poly(ethylene-1-octene) sample when the co-monomer content was increased to 3 mol% or higher; however, they observed that interpretation of their data was complicated by the concurrent breakdown of the lamellar morphology at higher co-monomer contents, which also increases the interfacial volume within the materials. Based on studies of poly(ethylene-1-octene), Bensason et al[4] correlated increasing SCB content with lower crystallinity and density, and furthermore divided the copolymers into several types, according to the observed morphologies. Below about 4 mol% SCB, lamellar crystallites and spherulitic morphologies were observed, typical of HDPE; above this level of SCB, a transition was observed to smaller, bundle-like or fringed micellar crystallites typical of elastomeric polyethylenes, and the spherulitic morphology broke down. It has been observed that the methyl and, to a lesser extent, ethyl branches can be included in the crystallites, due to their small sizes, while propyl and longer branches are completely excluded.[5–8] Using solid state NMR, White and co-workers[9] also reported an increase in the interfacial content (i.e. "constrained amorphous" plus "mobile all-trans" fractions) with increasing co-monomer content. By contrast, a similar solid state NMR study by Wang et al.[10] using LLDPEs with 1-octene co-monomers, prepared by single-site (ss) or Ziegler-Natta (ZN) catalysts, reported a decrease in the relative amount of interfacial content with increasing co-monomer content. Interestingly, at a relatively low co-monomer content, authors found branches to be uniformly distributed between the interphase and amorphous phases for both LLDPEs, while at high co-monomer content branches were found to be more populous in the amorphous phase than in the interphase for the ZN-LLDPE; the latter was attributed to the non-uniform distribution of co-monomer among chains of different length produced by the ZN catalyst. Experiments[11–13] have also shown that the regu-

lar unit cell structure of the crystal can be distorted by the presence of branches. Incorporation of methyl branches and, to a lesser extent, ethyl branches into the crystal causes distortion of the unit cell. In addition, segregation of longer branches into the interfacial region has been invoked to explain thinning of the crystal lamella and thickening of the interface[3] as well as deformation of the crystal lamella, as a result of surface stresses, for branches longer than ethyl.[11]

The presence of branches on the carbon backbone is believed to affect the way chains arrange in the interlamellar region, with consequences for the mechanical properties of branched materials. For example, by relating the brittle fracture tensile stress to an area fraction of tie chains, Liu et al.[14] inferred an increase in the population of tie chains as the length of short chain branches increased. Wang et al.[15] measured the dichroic ratio by FTIR in stretched thin films, and associated the unrelaxed portion with tie chains in the interlamellar domain. They observed an optimal branch content at which the inferred tie chain concentration (unrelaxed orientation) was highest, and the tear resistance of the material was most anisotropic.

In order to model HDPE and LLDPE (with sufficiently low branch content) on the molecular scale, it is useful to envision the organization of lamellar crystallites and noncrystalline, interlamellar regions into "lamellar stacks"; these stacks in turn form the basic motif of the spherulitic morphology.[16] The interlamellar regions within these stacks comprise transition zones right next to the crystals, which exhibit relatively high density and orientational order that dissipate with distance away from the crystals, and an amorphous zone in the middle with melt-like density and no orientational order. The interlamellar region is characterized by the presence of (i) chain segments that span the interlamellar region and connect two crystals ("bridges"), (ii) segments that start from one crystal and loop back into the same crystal ("loops"), and (iii) segments that start from one crystal face and end in the interlamellar region ("tails"). Such topological features and

the alternation of crystalline and noncrystalline domains have formed the basis of most molecular level descriptions of the semicrystalline state.[17–21] We have previously proposed an Interphase Monte Carlo (IMC) method that samples the metastable thermodynamic equilibrium ensemble of conformations and topologies within the interlamellar domain, subject to the constraints of density and crystalline boundaries.[22–24] The method has been applied to linear HDPE [25,26] and to isotactic polypropylene, with good results.[27] More recently, representative structures generated by this method have been used as the starting point for large strain deformations of HDPE using nonequilibrium molecular dynamics.[28–30]

Meanwhile, there are relatively few computer simulations studies that look specifically at LLDPE. One of the earliest was that carried out by Mattice and co-workers,[31–33] using a lattice model. They observed a uniform distribution of branches that occupied a single lattice site, while branches that occupied two sites were observed to segregate near the crystal-amorphous interface. They attributed this segregation to a gain in conformational entropy when the longer branches were relegated to the interface. However, lattice models are limited in their ability to represent accurately the conformers and packing interactions of real systems over distances of only a few bonds, and the model of Mattice and co-workers did not capture the difference in density between the crystalline and noncrystalline regions. Zhang et al.[34] subsequently carried out molecular dynamics (MD) simulations of branched polyethylenes using a united atom (UA) model, with chains constructed to mimic material obtained using either ss or ZN catalysts. Upon quenching to 375K, they observed the formation of small crystallites in both cases. In the case of their ss-LLDPE, branches were found to distribute uniformly throughout the interfacial and amorphous regions, while in the case of their ZN-LLDPE, branches actually segregated mainly into the amorphous regions, away from the interfaces. Zhang et al.[34] also reported some influ-

ence of SCB on the tie chain population. However, the 10 ns simulations used to obtain those results were too short to observe the development of fully formed lamellae. Most recently, Nilsson and co-workers[35] reported a model of phantom chain segments between lattice sites on the lamellar crystal surface, and concluded that there exists an optimal branch content at which interlamellar connection in the form of short bridges and "trapped" entanglements was maximized.

In this paper we use the IMC method to examine the effect of SCB on the interlamellar structure of LLDPE, subject to the conditions of metastable thermodynamic equilibrium previously used to model HDPE. We examine systems with three different branch lengths, corresponding to methyl, ethyl and butyl branches, at a fixed co-monomer content, crystallinity, and molecular weight. Our results for these systems are compared with those for linear, unbranched HDPE. Particular attention is paid to the effects of branching on conformation, and to the distribution of branch sites within the noncrystalline region.

Method:

In previous studies our group has used the force field developed by Paul, Yoon and Smith (PYS) [36], with modifications as described by In 't Veld et al,[24] to model molten and semicrystalline polyethylene (PE). The PYS force field was originally developed for short n-alkanes and was subsequently modified to capture static and dynamic properties of long n-alkane melts.[37,38] It has been shown to yield reasonable estimates for a number of relevant thermodynamic and mechanical properties, such as the melting temperature and enthalpy of fusion of n-alkane rotator phases[39–41] and the thermal expansion coefficients and elastic moduli of semicrystalline linear PE.[26] However, this force field lacks parameters for the methine carbons, where branches join the main backbone of the polymer chain. For this reason, we instead used the TraPPE-UA force

field to represent the interphase of both linear and branched polyethylenes in this work. The TraPPE-UA force field was originally developed to model the liquid-vapor saturation properties of small organic molecules.[26] The details of the TraPPE-UA force field can be found elsewhere.[42] We previously used this force field in a study of semicrystalline isotactic polypropylene.[27] In accord with that earlier work,[27] we replaced the fixed C–C bond length of the original TraPPE-UA force field with a quadratic potential, having force constant k_{eq}=3.761 MJ/(mol nm^2) and equilibrium bond length l_o = 0.154 nm. Recently Ramos et al [43] compared the PYS and TraPPE-UA force fields for the calculation of properties of linear PE melts and glasses, and crystallization. They concluded that both force fields perform adequately, but that the TraPPE-UA performed somewhat better in reproducing certain experimentally observed properties of the linear PE melt. In particular, the experimentally observed density and thermal expansion coefficient were found to be reproduced better using TraPPE-UA than PYS, while PYS results were in better agreement with experimentally observed values for characteristic ratio and coil dimensions. Both force fields predicted glass transitions that were in reasonable agreement with the available experimental data, but the TraPPE-UA force field was found to exhibit faster dynamics than PYS, as measured by, e.g., the Rouse times, dynamic structure factors, and self-diffusion coefficients. With regard to crystallization kinetics and semicrystalline structure and properties, however, the comparison of TraPPE-UA and PYS force fields was incomplete. In the current work, results for linear PE using both PYS and TRaPPE-UA are reported, for purposes of comparison to our previous work as well as to that of Ramos et al.[43]

The interlamellar domain was modeled using a similar strategy as described in our previous publications.[25] We started with a crystal phase, modeled using 48 linear polyethylene segments, each having 112 UA sites in fully extended conformation, placed on a crystal lattice of 4 x 6 x 56

unit cells so that the crystal exhibits pseudo-hexagonal symmetry. The crystal lattice was oriented such that the {201} facet of the crystal was normal to the z direction of the simulation cell.[26] Periodic boundary conditions were employed in all three directions, with covalent bonding across the boundary in the chain direction so that the polyethylene chains were effectively infinite in length. Finite molecular weight was introduced by selecting sixteen chains at random to form N_e=32 chains ends. The ten UA sites in each chain closest to the top and bottom boundaries of the simulation box were immobilized at their crystallographic positions to create a static crystal layer. Based on a simple mass balance and anticipating the subsequent addition of short chain branches, a number of sites were removed from each of the chain ends in order to ensure a final density of approximately 0.8 g/cm^3 within the 8.5 nm layer of material between the static crystal layers. Sato et al.[44] have measured the PVT properties of several random copolymers using dilatometry, and found that the density of the melts decreased slightly with increasing branch length. Upon extrapolation to T=350 K and P=1 atm, the melt densities for systems having 19, 10 and 3.5 mol% of 1-propene, 1-butene and 1-hexene co-monomer, respectively, were found to lie between ~0.80-0.83 g/cm^3, and to vary little with branch content in the range of interest for this study.[44]

This system of reduced density containing linear chains was then "amorphized", using an essentially athermal Monte Carlo simulation at a relatively high temperature of T = 10000 K, followed by subsequent annealing in stages at intermediate temperatures of T = 5000, 2000, 1000, 750, 500, 400, and 350 K. Short chain branches were then inserted to the final configurations thus obtained at T=350K, by attaching to backbone carbons randomly selected within the middle layer. A branch content of 5 branches per 100 backbone carbons was used for all of the systems. Assuming 50% crystallinity and no branches within the crystal lamellae, this level of branching

corresponds to 2.5 mol% SCB overall. The co-monomer content used in this work was somewhat higher than that used in most of the contemporary experimental studies, but was chosen to ensure good statistics for branch-related properties. To reduce atomic overlap resulting from the insertion of branches, branches were attached to the polyethylene backbone using a configuration-biased algorithm described in more detail below. In each of the branched systems simulated, the branches were exclusively methyl, ethyl, or butyl side chains. During the Monte Carlo simulations, branches were excluded from the static crystal region. The resulting models contained 4376, 4402, 4348, or 4397 UA sites for the linear, methyl-branched, ethyl-branched, and butyl-branched cases, respectively; the effective average molecular weight was ~10,000 g/mol. The dimensions of the simulation box were 3.69, 2.67, and 11.8 nm in the x, y and z directions for all of the systems. As discussed in the Introduction, although some experimental studies report a detectable amount of methyl or ethyl branches in the crystal region, any distortion of the crystal lattice as a result of such branching is assumed to be negligible here.

Simulations were conducted in an NN_eN_bVT ensemble, where the total number of sites N, number of (methyl) chain ends N_e, number of (methine) branch sites N_b, volume V, and temperature T were fixed. The simulations employed a mix of local rearrangement and connectivity altering moves to sample the relevant configurational phase space, as described in detail in previous papers.[25,26] The local rearrangement moves consisted of single site displacements, end rotations, and re-bridging moves. Connectivity altering moves included end-bridging and reptation moves. In addition, a new "branch move" was introduced, as described below, to ensure that branch locations could appear anywhere within the simulation (spatially unbiased) or at any point along the length of a loop, bridge or tail (topologically unbiased), with their distributions determined solely by reduction of free energy. Due to the presence of branch points, re-bridging,

end-bridging and reptation moves were forbidden for the parts of chains containing one or more branches. However, this restriction should not affect the ultimate state of equilibrium because every site along the chain backbones has a finite likelihood of being unbranched, due to the branch move.

The branch move allowed relocation of branches anywhere along the backbone of a segment or to the backbones of different segments. As shown in Fig. 1, a branch point C_i was selected at random, and the attached branch segment was excised. Next, a backbone CH_2 site C_j was selected at random for the new branch location. Chain ends (methyls), other branch sites (methines), and all carbons not part of a segment backbone were excluded from selection as the new branch site. The move also required mutation of the backbone CH site (C_i in the schematic Fig. 1) to a CH_2 at the old location and mutation of a backbone CH_2 site ("C_j" in the schematic Fig. 1) to CH at the new location. In order to avoid significant overlaps at the new branch location, which would lead to high energy and low percentage acceptance of the move, we used the Continuum Configurational Bias (CCB) algorithm[45] to "grow" the branch. Using this algorithm, the branch segment was created one site at a time. For each site, *k* trial configurations were generated, as depicted in Fig. 1.

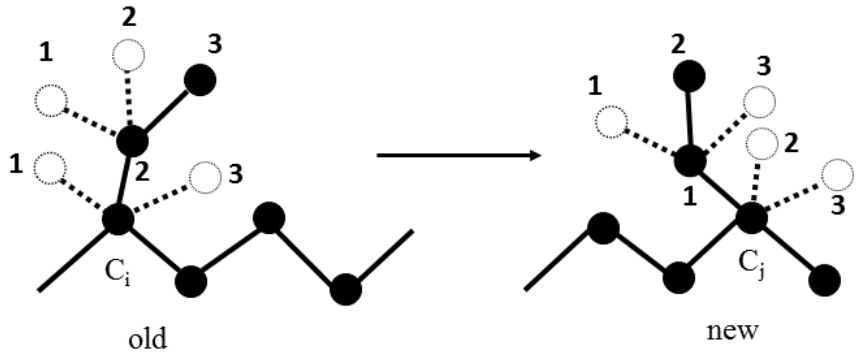

Figure 1: Schematic illustration of the CCB branch move.

In our work, these trial configurations were drawn from the biased distributions for bond length, bond angle and bond torsion with the preceding sites in the branch.[46] From these *k* trial configurations, one trial was selected according to the Boltzmann weight associated with the non-bonded interactions (only) of the site,

$$p_i = e^{-\beta U_{nb,i}} \Big/ \sum_{j=1}^{k} e^{-\beta U_{nb,j}} \quad . \tag{1}$$

The selected site was added to the branch, and the process was repeated until all of the sites in the branch were created. Growing the branch site-by-site in this fashion introduced a bias that must be removed by including the corresponding Rosenbluth weight[47] in the final acceptance criterion for the trial branch,

$$\mathrm{p_{acc}} = \min\{1, \frac{W_{new} \exp(-\beta U_{nb}^{new})}{W_{old} \exp(-\beta U_{nb}^{old})}\} \tag{2}$$

where $W = \prod_{i=1}^{l} p_i$ and l was the number of sites in a branch segment. The Rosenbluth weight for the old branch position was computed by taking the product of probabilities p_i for k–1 trial configurations along with the original positions of the sites in the branch segment. Note that the non-bonded interactions in the acceptance criteria also included the LJ interaction due to the mutation of both the old and new branch sites. In this work, a value of k=6 was used, as recommended by Ramos et al.[48] For a typical production run at T=350K, the acceptance ratio of the branch migration move for systems containing methyl, ethyl or butyl branches was 0.48, 0.20 or 0.03, respectively.

All of the results shown here correspond to T=350K, consistent with past reports using this method.[28,29]A typical equilibration run consisted of 40,000 MC cycles, and a typical production run consisted of 60,000 MC cycles. One cycle consists of 1086 Monte Carlo trial moves. Results were sampled once every MC cycle and averaged over ten independent simulations. Single-site displacement, end rotation, re-bridging, end-bridging, reptation, and CCB branch migration moves were selected at random, according to the proportions (out of 100): 47:15:14:14:7:3.

Results and Discussion:

Fig. 2 shows the density profiles along the z-axis for the systems examined in this work. The density profiles were obtained by calculating the volume contribution of each UA to the bins along the z-direction, using a procedure described in a previous paper.[23] The decay in density in the interfacial region for the branched systems was sharp compared to that for the unbranched system. This density decay depends on the local packing of the chains near the crystal surface and also on the "chain flux" through the interface, which in turn is governed by the populations

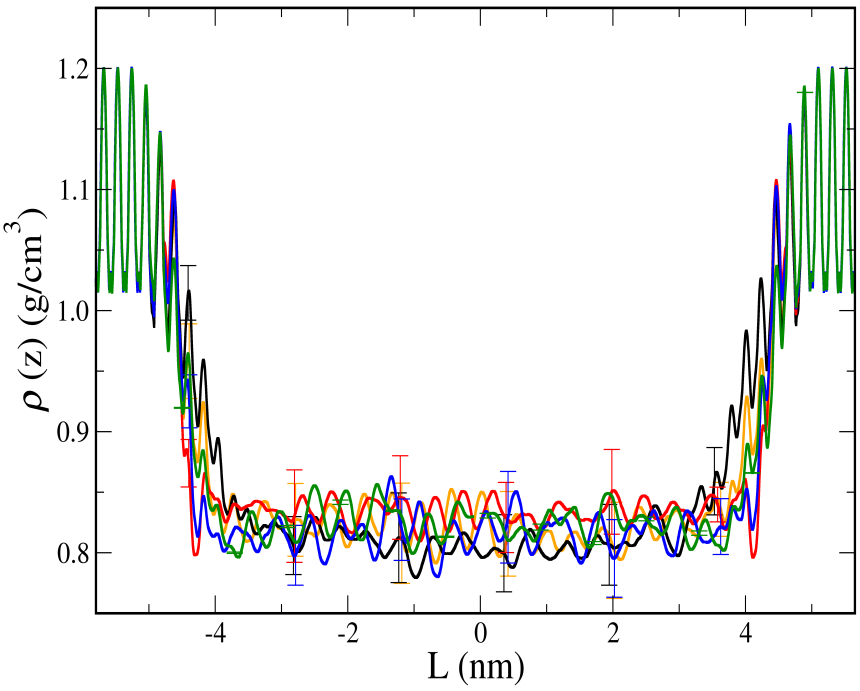

Figure 2: Profiles of mass density. Linear (black), methyl-branched (red) ethyl-branched (blue), and butyl-branched (green) systems were modeled using the TRaPPE-UA force field. The linear (orange) system was modeled using the PYS force field. Standard deviations are indicated at select points.

of short tails (whose ends lie in the interfacial zone) and short loops that fold tightly back into the crystal. When comparing branched systems, we observed little difference in the interfacial density profiles for the methyl and ethyl systems, while for the butyl system the density within the interfacial region was slightly higher than in the other branched systems. The density profile within the interface for the linear PE system using the TraPPE-UA force field was slightly higher than that obtained using the PYS force field, while the density in the fully amorphous region was cor-

respondingly a few percent lower, consistent with the results of Ramos et al for the amorphous melts.[48]

In Fig. 3 we present the orientational order (P_2) profile along the z-axis for all of the systems. The orientational order parameter P_2 of an atom is defined as the second Legendre polynomial of $\cos\theta_{iz}$, where θ_{iz} is the angle formed by the z-axis and the chord vector joining bonded neighboring atoms of site i along the backbone. P_2 evolves from a high value of 0.55, representative of the ordered crystal-like structure with chains tilted about 33° from the z-axis, consistent with the {201} crystal face, to P_2=0, representative of a completely disordered amorphous melt phase. The order profiles in the crystal and melt regions were similar for all of the systems. Like the density profile, a sharper decay in the orientational order profile was observed for the branched systems compared to the linear PE. This decay in orientational order profile is governed by the local conformations adopted by the chains near the crystal surface, with gauche states being responsible for the most dramatic reductions in orientational order. The order profile of linear PE using the TraPPE-UA force field closely resembled the profile obtained using the PYS force field.

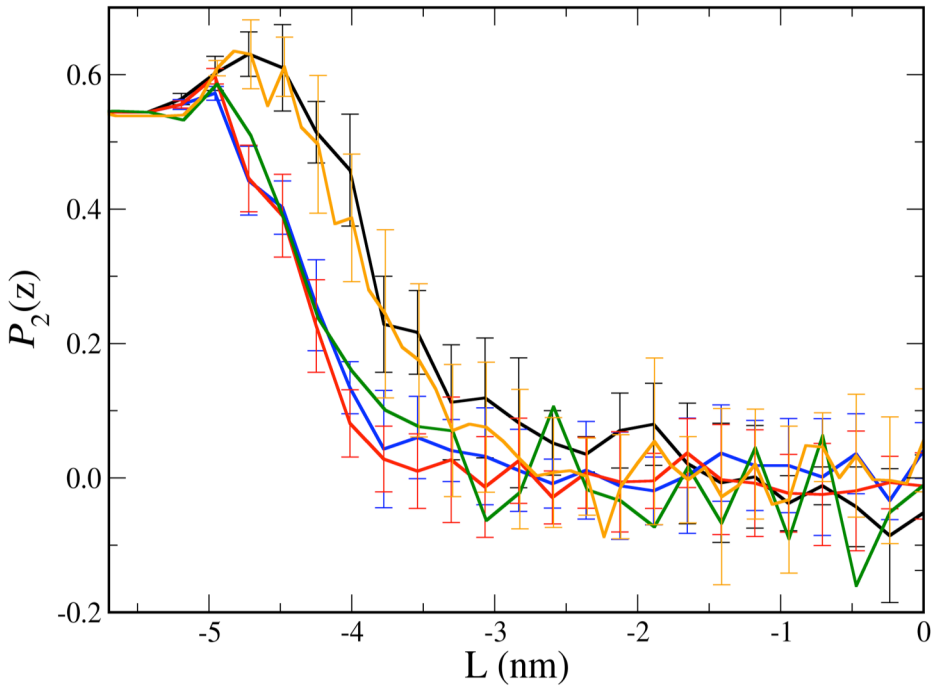

Figure 3: Orientational order parameter (P_2) profiles. The color scheme is the same as that used in Fig. 2. For improved statistics, the profile is mirrored about the mid-plane, and only a half section of the profile extending to the mid-plane in the amorphous melt region is shown in Fig. 3.

The decays in the interfacial density and orientational order profile were used to calculate the interfacial thickness of the semicrystalline material.[26] The computation of interfacial thickness using density decay was based on the Gibbs dividing surface (GDS), and the interfacial thickness was defined as twice the distance of the GDS from the first layer of static crystal sites.[26] The interfacial thickness obtained from the orientational order profile was computed by fitting a hyperbolic tangent curve to the profile as described in a previous report.[49] For consistency with the GDS method for density, the interfacial thickness was computed as twice the distance of the inflection point of the fitted hyperbolic tangent function from the first static layer

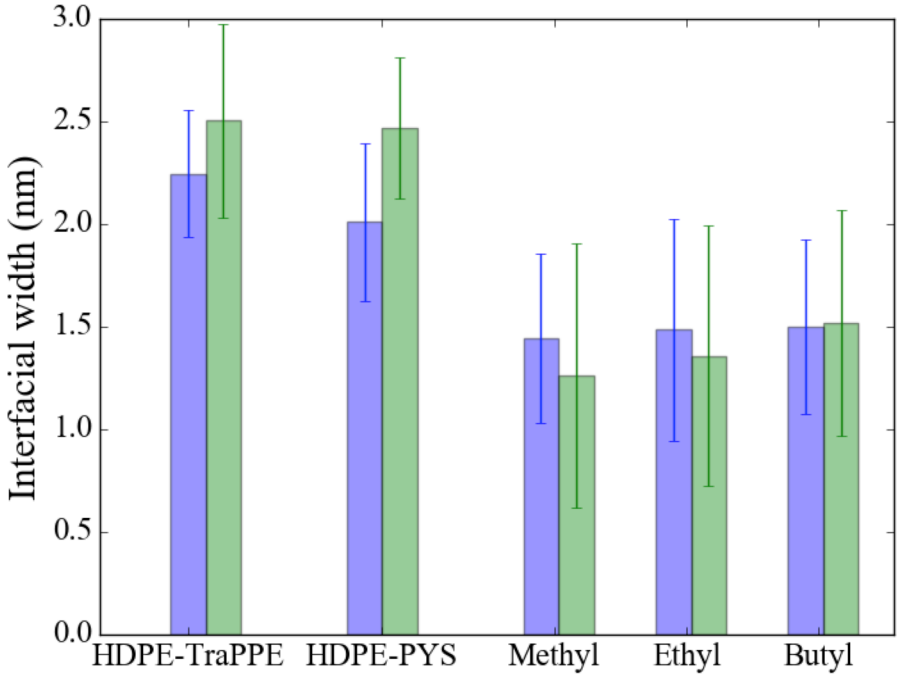

Figure 4: Interfacial thickness. Blue and green bars correspond to the thicknesses obtained from mass and orientation order profiles, respectively. See text for details. Standard deviations included.

of sites in the crystal. As shown in Fig. 4, the interfacial thicknesses obtained from the orientational order profiles exhibit similar trends compared to the interfacial thicknesses computed from the density profiles. The GDS-based interfacial thickness of the methyl-, ethyl- and butyl-branched systems was ~34 % lower than the corresponding linear (unbranched) system. The PYS and TraPPE-UA force fields produced statistically equivalent interfacial thicknesses for the linear system. The interfacial thickness of the linear system using the PYS force field was found to be 2.01±0.38 nm, slightly larger than that reported previously. This difference is due to the smoothing procedure used to obtain density profiles in the previous paper.[26]

In order to deduce how SCB affects the chain conformations of the semicrystalline material, we have computed the torsion angle distribution for the polymer backbone. This computa-

tion was performed separately for the torsions about bonds that included a methine site and those that did not. Fig. 5a presents the torsion angle distribution for the "linear" torsions about bonds between methylenes in the ethyl-branched case. As expected, according to the Boltzmann distribution, the trans states were more populated than the gauche states for the "linear" case. Fig. 5b presents the torsion angle distribution for the "branched" torsions about bonds involving a methine. The presence of branches causes gauche states to be more populated than the trans state at these sites. A decrease in the trans fraction along the backbone due to SCB has also been also observed in simulations of polymer melts.[50]

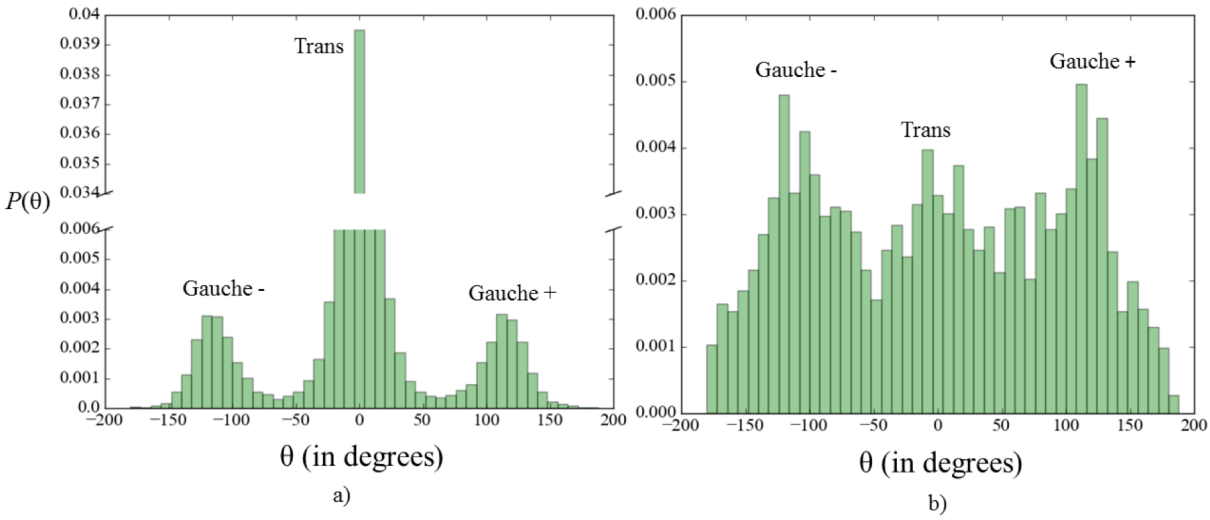

Figure 5: Torsion angle distributions for the ethyl-branched system. a) Torsion angle distribution for bonds between methylenes; b) torsion angle distribution for bonds involving a methine.

Next we look at the branch-specific orientational order profiles. Specifically, we compute P_2 of the methine carbons ("branched") and of the rest of the sites ("linear") separately. Fig. 6

shows the P_2 order profile versus z for branched and linear sites in the ethyl-branched case. The chain backbone directions at the branched sites are less aligned with the z-axis at the interface compared to the backbone direction elsewhere in the segments. The presence of a larger gauche fraction and a lower P_2 value due to branches demonstrates that branches induce local disorder along the backbone. This also explains the rapid decay of orientation order profiles within the interfaces in the branched systems.

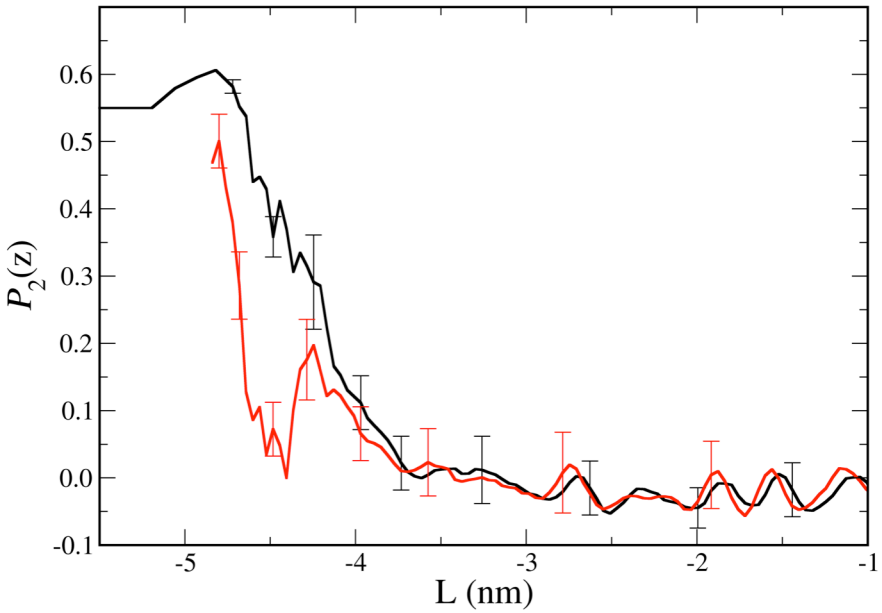

Figure 6: Orientational order (P_2) profiles for the ethyl-branched system according to site type: branched, or methine, (red) and linear, or methylene, (black) sites. Standard deviations are indicated at select points. For the branched sites, no branches were found for z axis values < -5.3 nm. Similar to the P_2 profile in Fig. 3, only a section of the profile is shown here.

Next we turn our attention to the question whether branches distribute uniformly in the interlamellar region or segregate preferentially to the interface. Fig. 7 shows the distribution of me-

thines in the interlamellar region for the branched systems. The branches appear to be distributed uniformly in the interlamellar region for all the branch lengths examined here. Right next to the crystal face one observes a systematic *decrease* in the concentration of methines as the branch length increases from methyl to ethyl to butyl. As branches become longer and bulkier, they take up more volume, excluding the methines to locations farther removed from the crystal face. We also speculate that with increasing branch length it becomes progressively more unfavorable energetically for branches to be present in short tails and loops, versus their longer counterparts. This speculation is based on the relatively high local density at the interface, which could favor the segregation of the smaller methines to the interface for energetic reasons; however, each methine is accompanied by a larger methyl group at the end of the branch, which is apparently unfavorable energetically, and more than compensates for the methine effect. Entropic effects prevail throughout the rest of the interlamellar domain, leading to a more or less uniform distribution of methines. Thus, the observed uniform distribution of branches in the interlamellar region in this model is a result of a complex interplay between the energetic and entropic factors present in the system under the imposed conditions of constrained equilibrium.

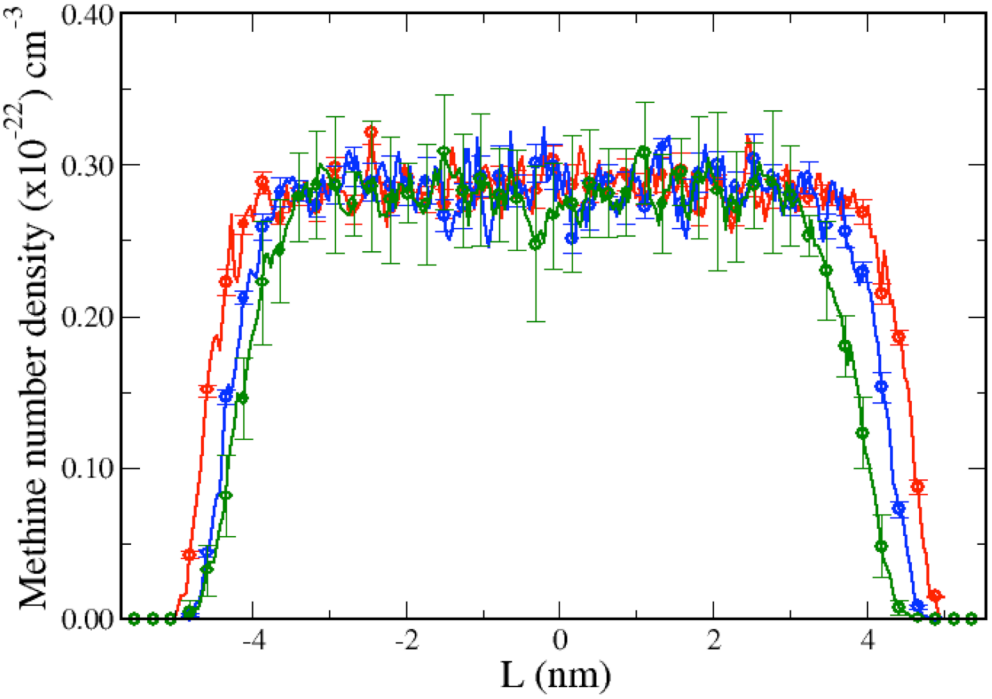

Figure 7: Distributions of branches in the interlamellar region: methyl-branched (red), ethyl-branched (blue), and butyl-branched (green). Standard deviations are indicated at select points.

Fig. 8 shows the probability distributions for the lengths of the loop, tail, and bridge populations for all of the systems. The qualitative features of the loop and tail distributions are similar. In Fig. 8a and 8b, the slopes of the curves are initially steep, and change rapidly for loops and tails shorter than 350 and 100 sites, respectively; for longer loops and tails, the distributions decay exponentially with N_{site}. Far from the crystal face, long loops and tails occupy the relatively low density of the amorphous region, and are free to adopt conformations similar to an unconstrained amorphous material. Hence for long loops and tails, the probability distribution is linear when plotted in semilogarithmic format. The slope in this linear regime is the excess chemical

potential associated with the addition of a site to a chain segment in an amorphous melt.[27] Close to the crystal face, the short loops and tails are constrained to lie within the interfacial region, where the density is higher; this high packing density results in a larger excess chemical potential per site, and thus a stronger length-dependence; loops and tails that are shorter than about 15 and 8 sites, respectively, were precluded based on microscopic reversibility considerations, since segments shorter than this cannot participate in rebridging moves. Fig. 8a indicates that there are differences in the loop distributions for linear and branched systems when $15 < N_{site} < 320$. Loops in this intermediate range are apparently more likely in HDPE than in the branched systems. By contrast, the tail probability distributions for all the systems studied here are very similar. The value of μ_{site} obtained from the slope of the tail distribution is ~ -0.024 kJ/mol and is similar to the value obtained from loop distribution. The value is close to the reported experimental value of -0.039 kJ/mol for linear alkanes obtained by fitting experimental data to the Peng-Robinson equation of state at T = 580 K and P = 1.02 atm.[51] For the linear PE cases, excellent agreement is observed between the length distributions of loops and tails for the PYS and TraPPE-UA force fields.

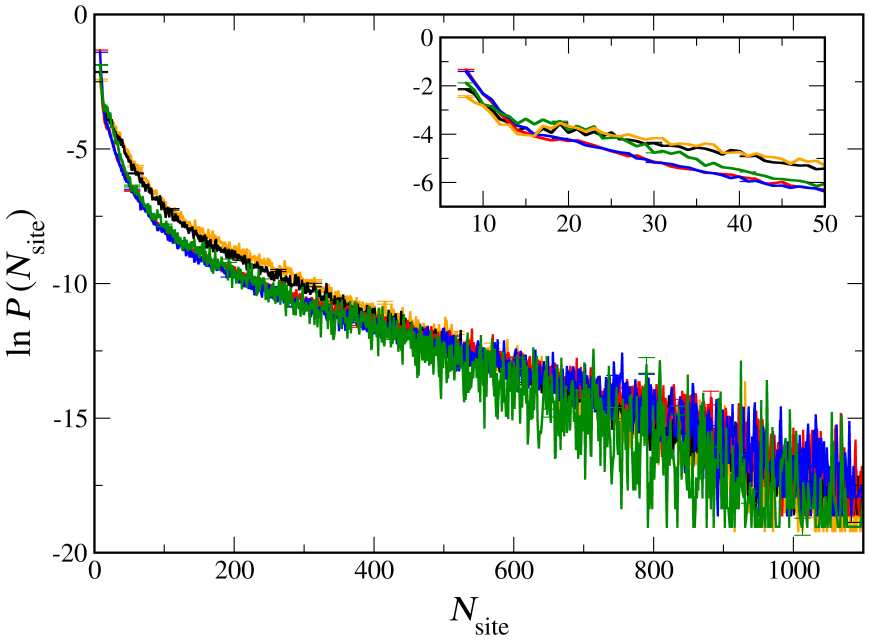

Figure 8(a)

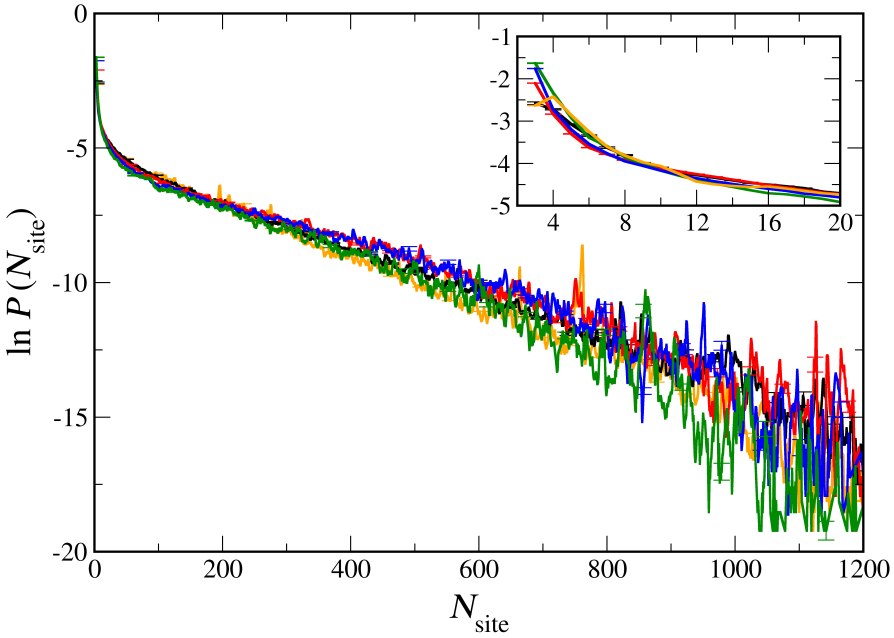

Figure 8(b)

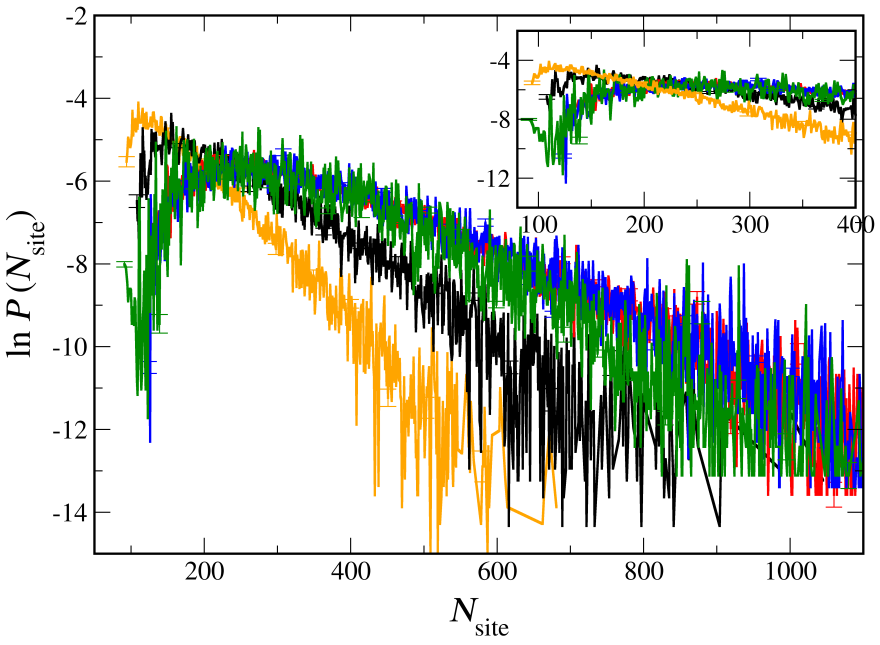

Figure 8(c)

Figure 8: Length distributions of (a) loops; (b) tails; (c) bridges. The color scheme is the same as that used in Fig. 2. Insets show the magnified distributions of the respective segment topologies.

Fig. 8c shows the probability distributions for bridge segments. These distributions are qualitatively different from the tail and loop distributions. The minimum length for a bridge is that required to span the interlamellar region by the shortest possible path, and thus is not much affected by the interface density but depends instead on the interlamellar thickness and the population of trans and gauche states. However, in agreement with the longer loops and tails, the distribution of bridges decays exponentially for long bridges. As a result, one observes a maximum in each of the distributions. Fig. 8c indicates that bridges shorter than about 100 sites are suppressed in all of the systems (too short to span the interlamellar domain). Significantly, bridges between 100 and 200 sites are suppressed in the branched systems relative to the linear one; this

behavior is attributed to the propensity of SCB to introduce gauche states into the bridge segment conformations, thereby increasing the contour length of a segment required to span the interlamellar domain. This trend is reversed for bridges longer than $N_{site} > 210$. We also observe a noticeable difference in the slopes of the bridge distributions using the PYS and TraPPE-UA force fields; PYS also shows a slightly higher preference for relatively short bridges ($N_{site} < 130$).

Conclusions:

What emerges from the results of these simulations is a description of semicrystalline polyethylene with short chain branching in which branch sites (specifically, methines) are distributed randomly throughout the amorphous component of the noncrystalline region, and are even expulsed from the interfacial region to an extent that increases with increasing branch length. Also, the thickness of the interphase between the crystalline and amorphous regions in polyethylenes with short chain branches is, if anything, smaller than that observed in the linear HDPE. This observation is similar to that observed by Wang et al[10] in their experiments. This trend also appears to be consistent with the observations of Zhang et al[34] from MD simulations, but probably for very different reasons, since the distributions of branch points in the current work were determined by thermodynamic considerations, and not fixed by a certain topological distribution and short time kinetics. The observed trends are at odds with the lattice simulation results of Mattice et al [31–33] and with many proposed interpretations of experimental data. Many experimental researchers have interpreted their data as indicative of an increase in the interfacial content with branching. However, such interpretations are at odds with the current simulation results, and we believe there is good reason to exercise caution in interpreting the experimental results solely as increases in interfacial thickness. We observe that most of the existing experi-

mental conclusions derive from an increase in the volume fraction or mole fraction of interfacial material with increasing branch length and number. However, an increase in the interfacial volume fraction implies an increase in interfacial thickness only if the interfacial area remains constant, i.e. the material maintains its lamellar structure at the given co-monomer content. For the same crystallinity, if the lamellae are thinner but more numerous, or if the material transforms into a fringed micellar morphology, the interfacial volume fraction can increase solely due to an increase in the interfacial area, and no conclusions can be drawn with regard to interfacial thickness.

Having said that, the simulations reported here are predicated on a constrained thermodynamic equilibrium that does not include explicit constraints on the spatial distribution of branch sites. By contrast, the kinetic viewpoint for lamellar crystal growth in LLDPE supposes that lamellae form primarily by incorporating the longest segments between branch points into the crystal phase, and that the resulting lamellar thickness is determined by the length distribution of these longest segments.[16] The statistical nature of these segment lengths could be responsible for a degree of surface roughness that would show up as greater interfacial thickness. As a corollary to this viewpoint, branches are thought to be trapped in the interface as a consequence of exclusion from the crystal lamella during crystallization, resulting in their high concentration there. The current simulations do not assume that such trapping occurs, nor do they take into account any memory of the kinetics that might have given rise to such initially high concentrations. In this regard, the current simulations describe the thermodynamic limit attained after all such memory effects are lost; discrepancies with experimental observations may also serve as evidence for such residual memory effects in the experimental data.

We found that branches induce more conformational disorder within the backbone of the segments, and a preference for gauche states. Such an influence affects the length distributions of loops and bridges that LLDPE materials exhibit. We found the shortest bridges ("tie chains") to be less likely in LLDPE's than in HDPE. This observation, too, is at odds with experimental studies that indicate an increase in population of "tie chains" (short bridges) with branching.[14] The population of bridges is dependent on the interlamellar thickness, and further investigation is needed to examine the effect of interlamellar thickness on population distribution of chain topologies.

Results obtained using both TraPPE-UA and PYS for linear PE exhibited qualitatively similar trends and showed only minor quantitative differences. Ramos et al. showed that TraPPE-UA does a slightly better job than PYS in predicting experimental melt properties of the linear HDPE. In the current work, such points of comparison with experimental data were limited. As far as the semicrystalline material is concerned, this work shows that one can use either of the force fields to model semicrystalline HDPE.

Under mechanical deformation, LLDPEs behave as a thermoplastic semicrystalline material at low co-monomer content, while at higher contents, where the lamellar morphology transforms into fringed micellar structure, an elastomeric response is observed.[4] The pre- and post-yield behavior of semicrystalline LLDPE is known to evolve with the extent of branching. For instance, experimental samples during uniaxial compression show an inverse relationship between yield stress and co-monomer content.[52] LLDPEs also exhibit various degrees of post-yield strain hardening when the length and concentration of branches are varied. This evolution in mechanical properties with branching content is believed to be mainly a result of changes in the crystallite thickness and chain topological characteristics, such as "tie-chain" fraction of the

amorphous section. As our work provides evidence for the presence of higher interfacial area instead of higher interfacial thickness in branched materials, the role of morphology on the mechanical behavior of LLDPEs demands further investigation. There is little known about how interfacial area, interfacial thickness, and chain topologies in the amorphous region influence mechanical properties of LLDPE. Experimental studies that attribute higher mechanical strength (high fracture tensile stress values) to a larger population of "tie-chains" in LLDPEs overlook the role of bridging entanglements in these materials. Populations of chain topologies and entanglements are strongly correlated with the interlamellar thickness,[16] which evolves with morphology as branch content increases, further complicating the situation. In order to disentangle these factors, any study comparing chain topologies in HDPE and LLDPE should do so for samples with similar interlamellar thickness, which is difficult to achieve experimentally at the same level of undercooling. In the light of current work, we believe it is important to take into account the several changes brought by short chain branching in the interlamellar region to understand the mechanical behavior of LLDPEs completely. Computer simulations can play an important role in this regard, and our ongoing efforts are aimed towards addressing these issues.

References:

(1) Voigtmartin, I. G.; Alamo, R.; Mandelkern, L. A quantitative electron-microscopic study of the crystalline-structure of ethylene copolymers. *J. Polym. Sci. Part B-Polymer Phys.* **1986**, *24* (6), 1283–1302.

(2) Defoor, F.; Groeninckx, G.; Schouterden, P.; Vanderheijden, B. Molecular, thermal and morphological characterization of narrowly branched fractions of 1-octene lldpe .2. Study of the lamellar morphology by transmission electron-microscopy. *Polymer (Guildf).* **1992**, *33* (24), 5186–5190.

(3) Alamo, R. G.; Viers, B. D.; Mandelkern, L. Phase-structure of random ethylene copolymers - a study of counit content and molecular-weight as independent variables. *Macromolecules* **1993**, *26* (21), 5740–5747.

(4) Bensason, S.; Minick, J.; Moet, A.; Chum, S.; Hiltner, A.; Baer, E. Classification of Homogeneous Ethylene-Octene Copolymers Based on Comonomer Content. *J. Polym. Sci. Part B Polym. Phys.* **1996**, *34* (7), 1301–1315.

(5) Hosoda, S.; Nomura, H.; Gotoh, Y.; Kihara, H. Degree of branch inclusion into the lamellar crystal for various ethylene alpha-olefin copolymers. *Polymer (Guildf).* **1990**, *31* (10), 1999–2005.

(6) Hosoda, S.; Hori, H.; Yada, K.; Nakahara, S.; Tsuji, M. Degree of Comonomer Inclusion into Lamella Crystal for Propylene/olefin Copolymers. *Polymer (Guildf).* **2002**, *43* (26), 7451–7460.

(7) Perez, E.; Bello, A.; Perena, J. M.; Benavente, R.; Martinez, M. C.; Aguilar, C. Solid-state nuclear magnetic-resonance study of linear low-density polyethylenes .1. Ethylene-1-butene copolymers. *Polymer (Guildf).* **1989**, *30* (8), 1508–1512.

(8) Perez, E.; Vanderhart, D. L.; Crist, B.; Howard, P. R. Morphological partitioning of ethyl branches in polyethylene by c-13 nuclear-magnetic-resonance. *Macromolecules* **1987**, *20* (1), 78–87.

(9) Tapash, A.; Deslauriers, P. J.; White, J. L. Simple NMR Experiments Reveal the Influence of Chain Length and Chain Architecture on the Crystalline/amorphous Interface in Polyethylenes. *Macromolecules* **2015**, *48* (9), 3040–3048.

(10) Wang, M.; Bernard, G. M.; Wasylishen, R. E.; Choi, P. A Solid-State C-13 NMR Investigation of the Morphology of Single-Site and Ziegler-Natta Linear Low-Density Polyethylenes with Varying Branch Contents. *Macromolecules* **2007**, *40* (18), 6594–6599.

(11) Howard, P. R.; Crist, B. Unit-cell dimensions in model ethylene butene-1 copolymers. *J. Polym. Sci. Part B-Polymer Phys.* **1989**, *27* (11), 2269–2282.

(12) Baker, A. M. E.; Windle, A. H. The Effects of Branching and Fibre Drawing on the Crystal Structure of Polyethylene. *Polymer (Guildf).* **2001**, *42* (2), 651–665.

(13) Few, C. S.; Wagener, K. B.; Thompson, D. L. Systematic Studies of Morphological Changes of Precision Polyethylene. *Macromol. Rapid Commun.* **2014**, *35* (2), 123–132.

(14) Liu, T. M.; Baker, W. E. The Effect of the Length of the Short Chain Branch on the Impact Properties of Linear Low Density Polyethylene. *Polym. Eng. Sci.* **1992**, *32* (14), 944–955.

(15) Wang, M.; Li, N.; Choi, P.; Zhang, Y. A Study of the Intermolecular Branch Frequency Dependence of Tie-Chain Concentration in Single-Site Linear Low-Density Polyethylene Blown Films by a New FTIR Method. *Can. J. Chem. Can. Chim.* **2010**, *88* (3), 260–266.

(16) Strobl, G. R. *The Physics of Polymers: Concepts for Understanding Their Structures and Behaviour*; Springer, 1997.

(17) DiMarzio, E. A.; Guttman, C. M. Three Statistical Mechanical Arguments That Favour Chain Folding in Polymer Systems of Lamellar Morphology. *Polymer (Guildf).* **1980**, *21* (7), 733–744.

(18) Guttman, C. M.; DiMarzio, E. A. Rotational Isomeric Modeling of a Polyethylene-like Polymer between Two Plates: Connection To "gambler's Ruin" problem. *Macromolecules* **1982**, *15* (2), 525–531.

(19) Balijepalli, S.; Rutledge, G. C. Conformational Statistics of Polymer Chains in the Interphase of Semi-Crystalline Polymers. *Comput. Theor. Polym. Sci.* **2000**, *10* (1–2), 103–113.

(20) Nilsson, F.; Lan, X.; Gkourmpis, T.; Hedenqvist, M. S.; Gedde, U. W. Modelling Tie Chains and Trapped Entanglements in Polyethylene. *Polym. (United Kingdom)* **2012**, *53* (16), 3594–3601.

(21) Huang, Y.-L.; Brown, N. The Dependence of Butyl Branch Density on Slow Crack Growth in Polyethylene: Kinetics. *J. Polym. Sci. Part B Polym. Phys.* **1990**, *28* (11), 2007–2021.

(22) Balijepalli, S.; Rutledge, G. C. Molecular Simulation of the Intercrystalline Phase of Chain Molecules. *J. Chem. Phys.* **1998**, *109* (16), 6523–6526.

(23) Gautam, S.; Balijepalli, S.; Rutledge, G. C. Molecular Simulations Df the Interlamellar Phase in Polymers: Effect of Chain Tilt. *Macromolecules* **2000**, *33* (24), 9136–9145.

(24) In 't Veld, P. J.; Rutledge, G. C. Temperature-Dependent Elasticity of a Semicrystalline Interphase Composed of Freely Rotating Chains. *Macromolecules* **2003**, *36* (19), 7358–7365.

(25) Hutter, M.; in 't Veld, P. J.; Rutledge, G. C. Polyethylene {201} Crystal Surface: Interface

Stresses and Thermodynamics. *Polymer (Guildf)*. **2006**, *47* (15), 5494–5504.

(26) In ’t Veld, P. J.; Hutter, M.; Rutledge, G. C. Temperature-Dependent Thermal and Elastic Properties of the Interlamellar Phase of Semicrystalline Polyethylene by Molecular Simulation. *Macromolecules* **2006**, *39* (1), 439–447.

(27) Kuppa, V. K.; in ’t Veld, P. J.; Rutledge, G. C. Monte Carlo Simulation of Interlamellar Isotactic Polypropylene. *Macromolecules* **2007**, *40* (14), 5187–5195.

(28) Lee, S.; Rutledge, G. C. Plastic Deformation of Semicrystalline Polyethylene by Molecular Simulation. *Macromolecules* **2011**, *44* (8), 3096–3108.

(29) Kim, J. M.; Locker, R.; Rutledge, G. C. Plastic Deformation of Semicrystalline Polyethylene under Extension, Compression, and Shear Using Molecular Dynamics Simulation. *Macromolecules* **2014**, *47* (7), 2515–2528.

(30) Yeh, I.-C.; Andzelm, J. W.; Rutledge, G. C. Mechanical and Structural Characterization of Semicrystalline Polyethylene under Tensile Deformation by Molecular Dynamics Simulations. *Macromolecules* **2015**, *48* (12), 4228–4239.

(31) Mathur, S. C.; Mattice, W. L. Non-uniform distribution of short branches in two-dimensional simulations of the amorphous regions between 2 crystalline lamellae. *Macromolecules* **1988**, *21* (5), 1354–1360.

(32) Mathur, S. C.; Rodrigues, K.; Mattice, W. L. Influence of a few short branches on the amorphous region of a semicrystalline polymer - simulation on a cubic lattice. *Macromolecules* **1989**, *22* (6), 2781–2785.

(33) Rodrigues, K.; Mathur, S. C.; Mattice, W. L. Influence of polyethylene-like short-range intramolecular interactions on the segregation of short branches and growth of the interfacial region in simulations of lightly branched semicrystalline polymers.

Macromolecules **1990**, *23* (9), 2484–2488.

(34) Zhang, M.; Yuen, F.; Choi, P. Differences in the Solid-State Structures of Single-Site and Ziegler-Natta Linear Low-Density Polyethylenes as Revealed by Molecular Dynamics Simulation. *Macromolecules* **2006**, *39* (24), 8517–8525.

(35) Moyassari, A.; Mostafavi, H.; Gkourmpis, T.; Hedenqvist, M. S.; Gedde, U. W.; Nilsson, F. Simulation of Semi-Crystalline Polyethylene: Effect of Short-Chain Branching on Tie Chains and Trapped Entanglements. *Polym. (United Kingdom)* **2015**, *72*, 177–184.

(36) Paul, W.; Yoon, D. Y.; Smith, G. D. An optimized united atom model for simulations of polymethylene melts. *J. Chem. Phys.* **1995**, *103* (4), 1702–1709.

(37) Waheed, N.; Lavine, M. S.; Rutledge, G. C. Molecular Simulation of Crystal Growth in N-Eicosane. *J. Chem. Phys.* **2002**, *116* (5), 2301–2309.

(38) Waheed, N.; Ko, M. J.; Rutledge, G. C. Molecular Simulation of Crystal Growth in Long Alkanes. *Polymer (Guildf).* **2005**, *46* (20), 8689–8702.

(39) Yi, P.; Rutledge, G. C. Molecular Simulation of Crystal Nucleation from the Melt: N-Alkanes to Polyethylene. *Abstr. Pap. Am. Chem. Soc.* **2012**, *244*.

(40) Yi, P.; Rutledge, G. C. Molecular Simulation of Bundle-like Crystal Nucleation from N-Eicosane Melts. *J. Chem. Phys.* **2011**, *135* (2).

(41) Yi, P.; Rutledge, G. C. Molecular Simulation of Crystal Nucleation in N-Octane Melts. *J. Chem. Phys.* **2009**, *131* (13).

(42) Martin, M. G.; Siepmann, J. I. Novel Configurational-Bias Monte Carlo Method for Branched Molecules. Transferable Potentials for Phase Equilibria. 2. United-Atom Description of Branched Alkanes. *J. Phys. Chem. B* **1999**, *103* (21), 4508–4517.

(43) Ramos, J.; Vega, J. F.; Martínez-Salazar, J. Molecular Dynamics Simulations for the

Description of Experimental Molecular Conformation, Melt Dynamics, and Phase Transitions in Polyethylene. *Macromolecules* **2015**, *48* (14), 5016–5027.

(44) Sato, Y.; Hashiguchi, H.; Inohara, K.; Takishima, S.; Masuoka, H. PVT Properties of Polyethylene Copolymer Melts. *Fluid Phase Equilib.* **2007**, *257* (2), 124–130.

(45) de Pablo, J. J.; Laso, M.; Suter, U. W.; Cochran, H. D. Continuum Configurational Bias Monte-Carlo Studies of Alkanes and Polyethylene. *Fluid Phase Equilib.* **1993**, *83*, 323–331.

(46) Baschnagel, J.; Qin, K.; Paul, W.; Binder, K. Monte Carlo Simulation of Models for Single Polyethylene Coils. *Macromolecules* **1992**, *25* (12), 3117–3124.

(47) Rosenbluth, M. N.; Rosenbluth, A. W. Monte Carlo Calculation of the Average Extension of Molecular Chains. *J. Chem. Phys.* **1955**, *23* (2), 356–359.

(48) Ramos, J.; Peristeras, L. D.; Theodorou, D. N. Monte Carlo Simulation of Short Chain Branched Polyolefins in the Molten State. *Macromolecules* **2007**, *40* (26), 9640–9650.

(49) Ko, M. J.; Waheed, N.; Lavine, M. S.; Rutledge, G. C. Characterization of Polyethylene Crystallization from an Oriented Melt by Molecular Dynamics Simulation. *J. Chem. Phys.* **2004**, *121* (6), 2823–2832.

(50) Moorthi, K.; Kamio, K.; Ramos, J.; Theodorou, D. N. Monte Carlo Simulation of Short Chain Branched Polyolefins: Structure and Properties. *Macromolecules* **2012**, *45* (20), 8453–8466.

(51) Spyriouni, T.; Economou, I. G.; Theodorou, D. N. Thermodynamics of Chain Fluids from Atomistic Simulation: A Test of the Chain Increment Method for Chemical Potential. *Macromolecules* **1997**, *30* (16), 4744–4755.

(52) Kennedy, M. A.; Peacock, A. J.; Failla, M. D.; Lucas, J. C.; Mandelkern, L. Tensile

Properties of Crystalline Polymers: Random Copolymers of Ethylene. *Macromolecules* **1995**, *28* (5), 1407–1421.

Table of Contents Graphic for

"Effect of short chain branching on the interlamellar structure of semicrystalline polyethylene"

Vaibhaw Kumar, C. Rebecca Locker, Pieter J. in 't Veld, and Gregory C. Rutledge